Communications in Physics, Vol. 34, No. 2 (2024), pp. 179-191
DOI: https://doi.org/10.15625/0868-3166/19484

Study on optical properties of hexagonal lattice photonic crystal fibers infiltrated with heavy water

Trong Dang Van, Bao Tran Le Tran and Lanh Chu Van†

Department of Physics, Vinh University, 182 Le Duan, Nghe An Province, Vinh City, Viet Nam

E-mail: †chuvanlanh@vinhuni.edu.vn

Received 3 February 2024
Accepted for publication 29 May 2024
Published 6 June 2024

Abstract. *This paper analyzed a photonic crystal fiber (PCF) made from fused silica glass, with a core filled with heavy water. The PCF properties including dispersion, effective mode area, effective refractive index, and confinement loss of the proposed fibers were analyzed in detail. We determined two fiber structures possessing optimal dispersion with the lattice constant* (Λ) *and the filling factor as follows:* $\Lambda = 1.1\ \mu m$, $d/\Lambda = 0.92$ *for fiber #F_1 and* $\Lambda = 1.4\ \mu m$, $d/\Lambda = 0.92$ *for fiber #F_2. Fiber #F_1 operating in an all-normal dispersion regime has a pump wavelength of 800 nm. Proposed fiber #F_1 has a dispersion value of 44.68 ps.nm^{-1}.km^{-1}, effective mode area of 1.22 μm^2 and confinement loss of dB/m at the pump wavelength. Meanwhile, fiber #F_2 operates in an anomalous dispersion regime. At a pump wavelength of 850 nm, fiber #F_2 has a dispersion value of 10.6 ps.nm^{-1}.km^{-1}, an effective mode area of 1.92 μm^2, and a confinement loss of dB/m. The proposed fibers are designed based on cheap, common, and environmentally friendly materials. Furthermore, these proposed fibers provide flat dispersion, small effective mode area, and low confinement loss in the range of 10^{-15} to 10^{-16} dB/m which are the highlights of our model. From these advantages, the proposed fibers have been targeted for flat and smooth broadband supercontinuum generation for near-infrared applications.*

Keywords: photonic crystal fiber; confinement loss; dispersion; effective mode area; supercontinuum generation.

Classification numbers: 42.55.Tv; 42.60.Jf; 77.22.Gm.

1. Introduction

The creation of photonic crystal fibers (PCFs) was a breakthrough in fiber optic technology by Knight *et al.* [1]. PCFs with extremely unique optical properties that traditional optical

fibers cannot have such as endless single-mode guidance [2], dispersion control [3], and high birefringence [4], PCFs with a small core can show very high nonlinear properties [5]. These are important properties that are widely used in fiber optic technology.

One of the most important applications of PCFs is supercontinuum generation (SCG) [6]. SCG sources with special coherence, wide bandwidth, and strong brightness have a variety of potential applications, such as high-resolution microscopy [7], novel SCG laser that is all-fiber-integrated [8], mid-infrared supercontinuum tissue imaging [9], the developed fiber-laser source for fast micromachining, microfabrication, and microprocessor [10], and make an all-optical atomic clock [11].

Key quantities that have important effects on SCG include the effective mode area (A_{eff}), dispersion, loss, and nonlinear coefficient [12]. To achieve the best SCG efficiency, the PCF's chromatic dispersion curve should be flat and close to zero, and the loss and effective mode area should be as small as possible. Therefore, the PCF must be designed to achieve those characteristics. We can design and adjust the structural parameters of PCF to achieve that goal such as lattice constant, pore size, shape, solid or hollow core, and materials.

Scientists have tried to create effective SCG using solid-core PCFs with air holes filled with liquid or gas. For instance, Ranka *et al.*, studied SCG in optical fiber structure of silica-air [13]. Dudley *et al.*, studied SCG in air-silica microstructured fibers by both nanosecond and femtosecond pulse excitation [14]. Khoa *et al.*, studied SCG in the suspended-core optical fibers made of borosilicate of NC21A glass infiltrated with water [15], and Hieu *et al.*, studied SCG in PCF with the normal dispersion regime [16]. The advantage of this type of fiber is that it has a small mode area. However, the limitation of these fibers is that the nonlinear refractive index of the solid core is often small and the fiber loss is quite large.

Recently, a promising alternative using liquid-filled hollow-core fibers with high nonlinear refractive index and high transparency was investigated for efficient SCG. Fluid with a high nonlinear refractive index is injected into the core of the PCF to create a refractive index difference compared to the cladding. This helps light spread in the PCF follow the total internal reflection as in conventional optical fibers [17, 18]. Typical publications of these include SCG in liquid-core optical fibers [19], generation of coherent supercontinuum in toluene–core PCFs [20, 21], SCG in chloroform–core PCFs [22], SCG in nitrobenzene-core PCFs [23–25], SCG in CS_2 – core PCFs [27, 28]. These publications have produced effective SCG with flat dispersion characteristics but it still has some limitations such as the effective mode area and loss in these fibers are quite large [20–25, 27, 28]. That greatly affects SCG efficiency. Besides, the liquids used in the above analytical works are highly toxic and affect health when doing experiments.

To overcome the above limitations, in this paper, we analyzed hexagonal lattice PCFs made from fused silica glass, the core of which is filled with heavy water. The PCF characteristics of the fundamental mode are studied and optimized with the variation of structural parameters. Through this investigation, we have selected two optimal structures suitable for highly efficient SCG.

Based on collecting and analyzing many different liquids. We have identified a fluid that can optimize the effective mode area, dispersion, and loss and not affect human health: heavy water (D_2O). Heavy water and water (H_2O) are both interchangeable solvents. However, the hydrogen bonding strengths in H_2O and D_2O are different, resulting in distinct differences in physical properties such as density, viscosity, and thermal ability. Because deuterium atoms are heavier than hydrogen atoms, the amplitude of atomic vibrations is smaller and the deuterium

bonding in heavy water is stronger than hydrogen bonding in water. The refractive index also varies significantly: at 293 K and 589.3 nm, the refractive index of water is 1.33, while heavy water is 1.32 and in the wavelength range from 500 nm to 1200 nm, the absorbance coefficient of heavy water is very small compared to the absorption coefficient of water [29, 30]. The nonlinear refractive index of heavy water and water is approximately equal to m^2/W [31].

The article is structured as follows. Sec. 2 describes the numerically constructed heavy water core hexagonal lattice PCF. The next part is to analyze the characteristics of PCF with changes in structural parameters and propose the optimal structure for effective SCG. Finally, Sec. 4 presents the conclusions of the study.

2. Numerical modeling of PCF

We designed the geometrical structure of the PCF filled with heavy water, as shown in Fig. 1. The background material is fused silica (SiO_2), and the hollow core infiltrated with heavy water is surrounded by air holes constituting a photonic cladding. The cladding consists of eight rings of air holes of diameter d ordered in a hexagonal lattice with the lattice constant Λ. The diameter of the core is defined by the formula $D_c = 2\Lambda - 1.1d$. The filling factor of the cladding is defined as $f = d/\Lambda$. In the computer simulations, we used the following lattice constants Λ has been varied between 1.0μm to 1.4 μm in steps of 0.1 μm and the filling factors f has been varied between 0.92 to 0.96 in steps of 0.1. We choose a large filling factor to make the average refractive index of the cladding smaller than the refractive index of the core so that the light passing through the PCF follows the phenomenon of total internal reflection. This new point is very different from previous publications [20–25]. For the set of parameters selected for the structures, we used the Lumerical Mode Solutions software [26] and performed 25 simulations. The results obtained show that all PCF structures are single-mode.

Refractive index characteristics are modeled using Sellmeier's equation as given below, where the C_i coefficients have dimensions of micrometers squared (μm^2):

$$n^2(\lambda) = B_0 + \frac{B_1\lambda^2}{\lambda^2 - C_1} + \frac{B_2\lambda^2}{\lambda^2 - C_2} + \frac{B_3\lambda^2}{\lambda^2 - C_3}, \tag{1}$$

where λ is the wavelength and n is the real refractive index of the material. The Sellmeier's coefficients, B_i, for fused silica [31] and heavy water [28] are presented in Table 1. The effective refractive index is determined by:

$$n_{eff} = \frac{\lambda\beta}{2\pi}, \tag{2}$$

where β is the propagation constant.

Figure 2 shows a comparison of the refractive index of PCF materials. It can be seen that the refractive index of silica is larger than that of the heavy water used in the core. This is a new point compared to previous works using liquids with a higher refractive index than silica [20–25]. Light is still confined in the core according to the phenomenon of total internal reflection as analyzed above.

The absorption coefficient of heavy water is shown in Fig. 3. In the wavelength range from 0.5 μm to 1.2 μm , the absorption coefficient of heavy water is small. Therefore, we investigate the characteristics of PCF in the wavelength range from 0.5 μm to 1.2 μm to reduce loss to the lowest level in the light transmission process of PCF.

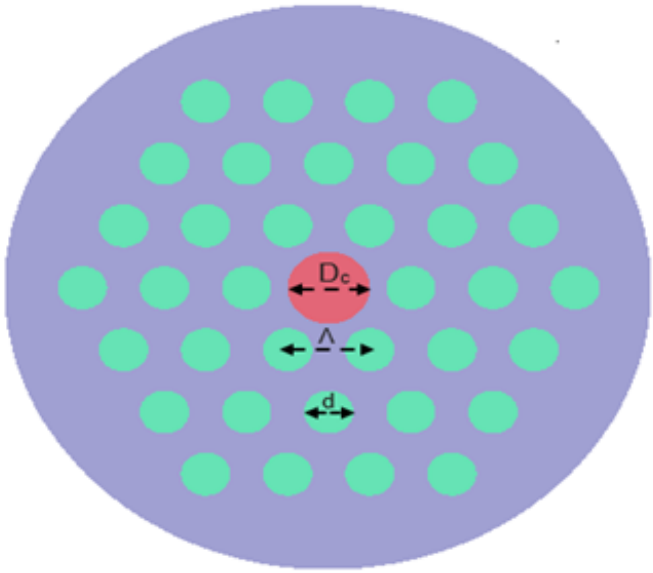

Fig. 1. The first three rings of cladding in the geometrical structure of the PCF are filled with heavy water. D_c is the diameter of the liquid-filled core, Λ is lattice constants and d is the diameter of the air-filled core.

Table 1. Sellmeier's coefficients for the materials used.

Sellmeier cofficients	Values	
	Fused Silica ($\mathbf{SiO_2}$)	Heavy Water ($\mathbf{D_2O}$)
B_0	1	1
B_1	0.6694226	-0.30637
B_2	0.4345839	0.74659
B_3	0.8716947	-
$C_1\ [\mu\mathrm{m}^2]$	4.4801×10^{-3}	-47.2669
$C_2\ [\mu\mathrm{m}^2]$	1.3285×10^{-2}	0.00893
$C_3\ [\mu\mathrm{m}^2]$	95.341482	-

Chromatic dispersion includes a waveguide and material dispersion. It is determined according to Eq. (3), where $\mathrm{Re}[n_{eff}]$ is the real part of the effective refractive index of a guided mode and c is the velocity of light in a vacuum.

$$D = -\frac{\lambda}{c}\frac{d^2\,\mathrm{Re}\,[n_{eff}]}{d\lambda^2}. \tag{3}$$

The nonlinear coefficient of PCF has the unit of $\left(\mathrm{W}^{-1}.\mathrm{km}^{-1}\right)$ determined by the following formula:

$$\gamma = \frac{\omega}{c}\left(\frac{n_2}{A_{eff}}\right) = \frac{2\pi}{\lambda}\left(\frac{n_2}{A_{eff}}\right), \tag{4}$$

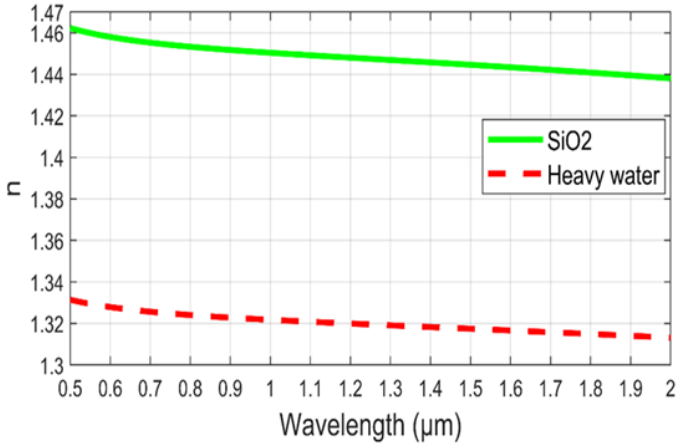

Fig. 2. Characteristics of the real part of the refraction index of heavy water [29] and fused silica [32].

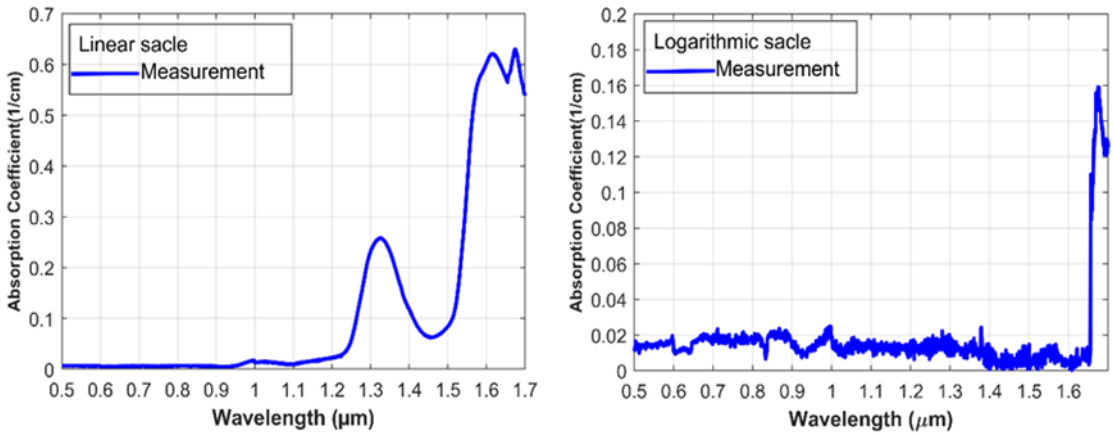

(a) (b)

Fig. 3. The absorption coefficient of liquid heavy water at a temperature of 20 °C on (a) linear and (b) logarithmic scale as a function of wavelength [29].

where ω is the angular frequency, and A_{eff} is the effective mode area (an important characteristic of PCF). It is inversely proportional to the nonlinear coefficient and is defined as follow [19]:

$$A_{eff} = \frac{\left(\int_{-\infty}^{\infty}\int_{-\infty}^{\infty}|E(x,y)|^2 dxdy\right)^2}{\int_{-\infty}^{\infty}\int_{-\infty}^{\infty}|E(x,y)|^4 dxdy}, \tag{5}$$

where E is the electric field amplitude.

3. Result and Discussion

3.1. The effective refractive index (n_{eff})

Figure 4 illustrates the change in the effective refractive index of the fundamental mode in PCFs with the filling factor (d/Λ) chosen between 0.92 and 0.96 and the lattice constant $(\Lambda) : \Lambda =$ 1.0 μm , $\Lambda = 1.1$ μm, $\Lambda = 1.2$ μm , $\Lambda = 1.3$ μm, and $\Lambda = 1.4$ μm. Based on the graph, we can see that the change of wavelength, d/Λ, and lattice constant (Λ) lead to a change in the effective refractive index. Specifically, as the wavelength increases, the refractive index decreases and has a similar shape for all cases. This behavior is mostly because the longer wavelength has a stronger capacity to penetrate within the cladding district of PCF than that of a briefer wavelength [34]. In addition, as the filling factor (d/Λ) increases, the effective refractive index decreases, and n_{eff} increases if the lattice constant (Λ) increases.

3.2. The effective mode area

Figure 5 shows the effective mode areas of the fundamental modes simulated for PCFs with varying structural parameters. At the same structural parameters, the effective mode area varies with wavelength and has the same shape. Specifically, with the same lattice constant and at the same value of wavelength, A_{eff} increases as the filling factor decreases. Meanwhile, as the lattice constant increases, the effective mode area increases at a certain filling factor and wavelength. A smaller effective mode area leads to a large nonlinear coefficient because it is inversely proportional through Eq. (4). Highly nonlinear PCF is the best condition for SCG with input energy as low as picojoules. The effective mode area in this work is much smaller than the effective mode area reported in liquid core PCF in previous projects [31,32]. The current values of the optimized fibers compared with previous works are shown in Table 2.

3.3. Dispersion

Figure 6 shows the effect of varying the filling factor (d/Λ) and the lattice constant (Λ) on the dispersion (D). Looking at the graph, the hexagonal lattice structure has dispersion that varies with different wavelengths. The dispersion curves obtained include anomalous dispersion with one or two ZWDs. The dispersion characteristic has been dominated by the change of the filling factor d/Λ and the lattice constant (Λ). Moreover, the change of these two parameters causes the ZDW to shift to a longer wavelength. Specifically, at lattice constants $\Lambda = 1.1$ μm and $\Lambda = 1.2$ μm (Fig. 6. a, b), anomalous dispersion with two ZDWs appears in all fibers with the investigated filling coefficients. When examining larger lattice constants (larger cores) with $\Lambda = 1.3$ μm (Fig. 6c) and $\Lambda = 1.4$ μm (Fig. 6d), the results show the anomalous dispersion with two ZDWs no longer appears but only the anomalous dispersion curve appears with one ZWD in these two cases. The structure parameter Λ also strongly influences the properties of dispersion, a huge change like the dispersion profile observed with a larger lattice constant. The dispersion characteristic is more controllable in smaller core PCFs because of their strong light confinement. From the above analysis, the dispersion characteristics can be controlled by changing the filling factor (d/Λ) of the first ring and the lattice constant (Λ).

Dispersion is one of the key factors for SCG, the flat dispersion fiber allows us to obtain a wider SCG [1]. Therefore, fiber structures with flat dispersion curves, near-zero dispersion curves, and ZDWs compatible with pump wavelength have always been the goal of dispersion optimization [1].

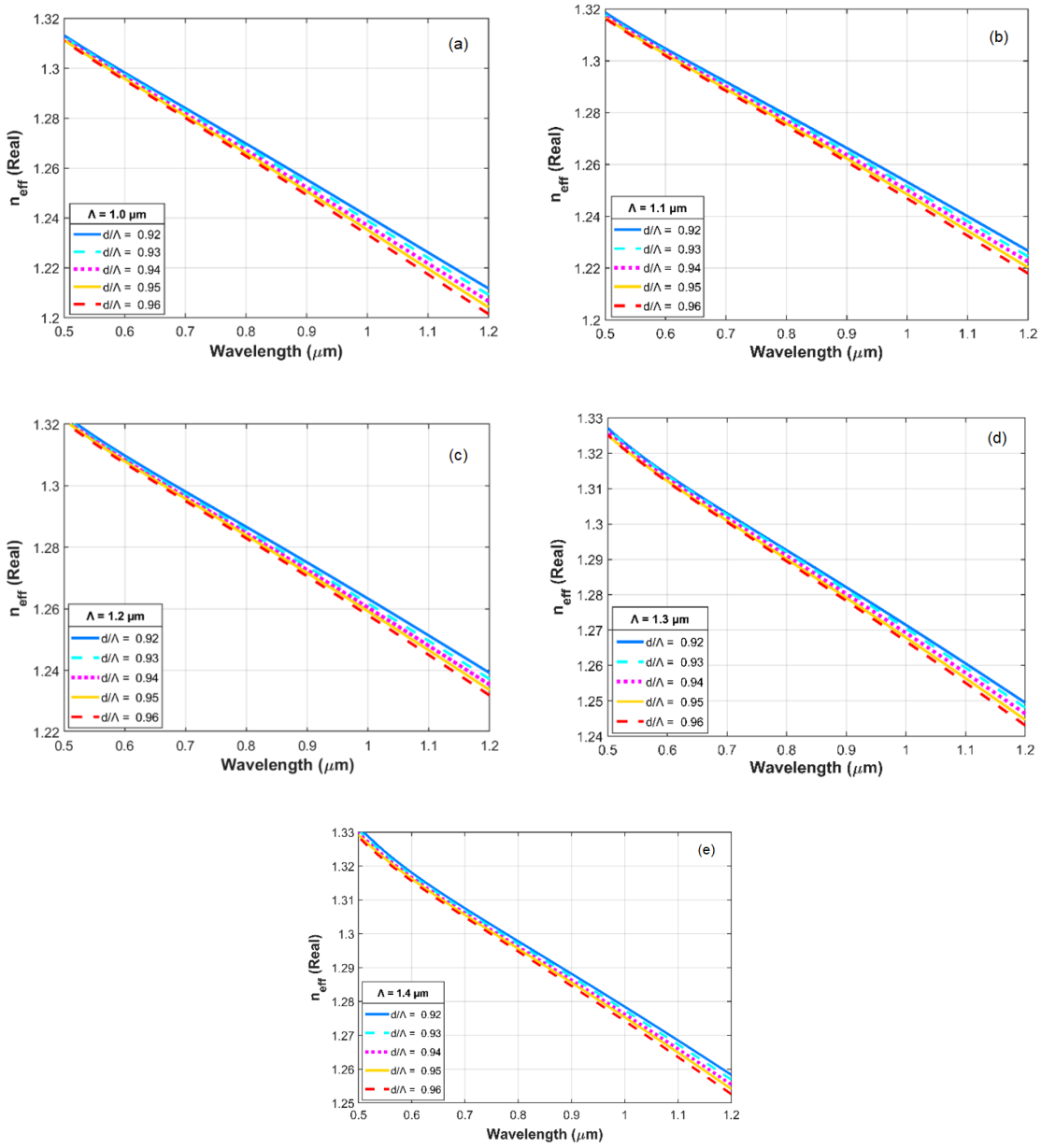

Fig. 4. The real part of the effective refractive index as a function of wavelength of PCFs with various d/Λ for (a) $\Lambda = 1.0$ μm , (b) $\Lambda = 1.1$ μm, (c) $\Lambda = 1.2$ μm, (d) $\Lambda = 1.3$ μm and (e) $\Lambda = 1.4$ μm.

Based on the analysis in the above section, we choose two optimal dispersion fiber structures named fiber #F_1 and fiber #F_2 (Figure 7. a). Fiber #F_1 has lattice constant $\Lambda = 1.1$ μm and filling factor $d/\Lambda = 0.92$, has two zero dispersion wavelengths ZDW_1 = 0.731 μm , ZDW_2

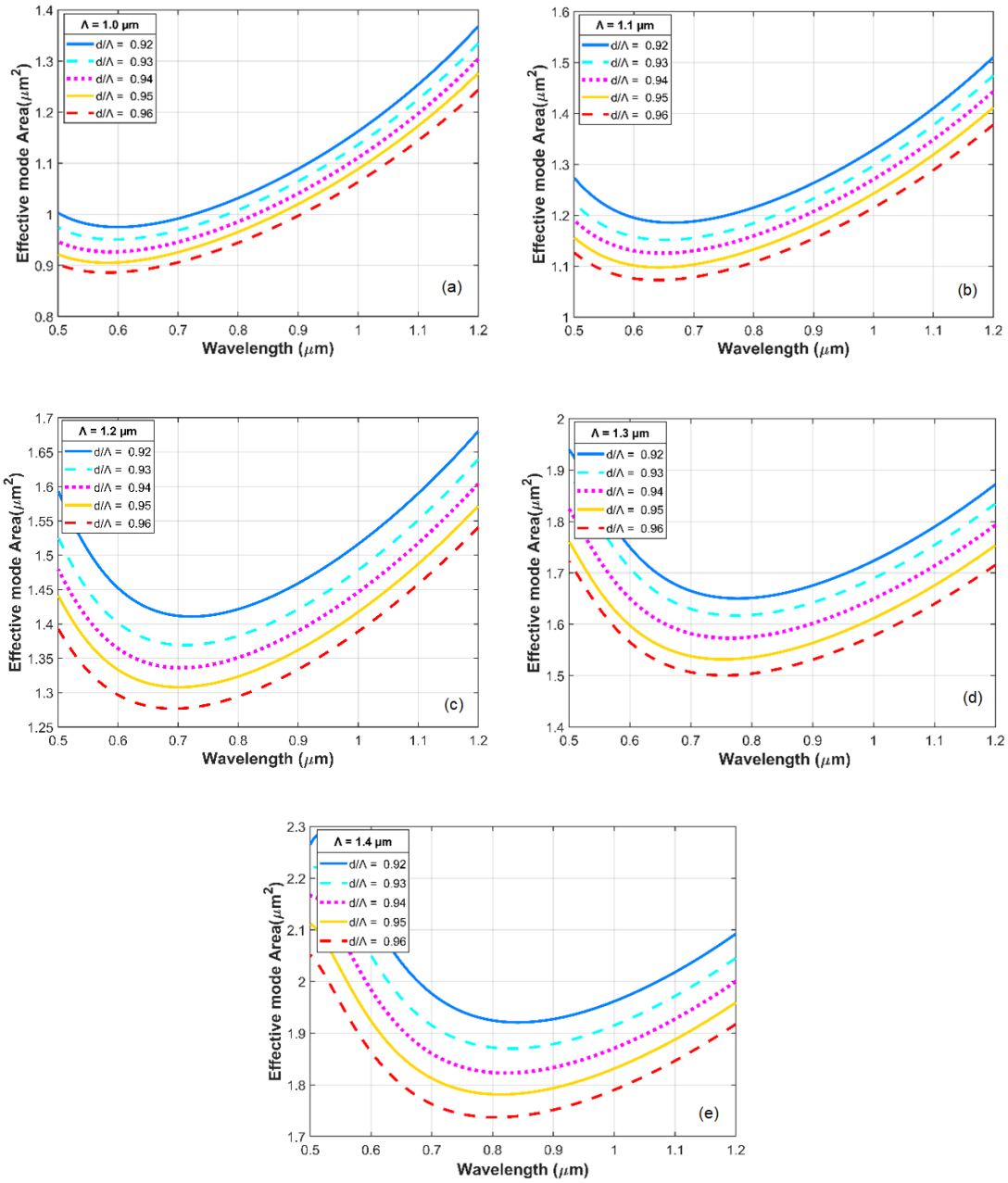

Fig. 5. The effective mode area as a function of wavelength of PCFs with various d/Λ for (a) $\Lambda = 1.0\ \mu$m , (b)$\Lambda = 1.1\ \mu$m, (c) $\Lambda = 1.2\ \mu$m , (d) $\Lambda = 1.3\ \mu$m and (e) $\Lambda = 1.4\ \mu$m.

= 1.149 μm . This fiber is intended for SCG in the anomalous dispersion regime with a pump wavelength of 800 nm. The dispersion is equal to 44.68 ps/nm/km at the pump wavelength. Fiber

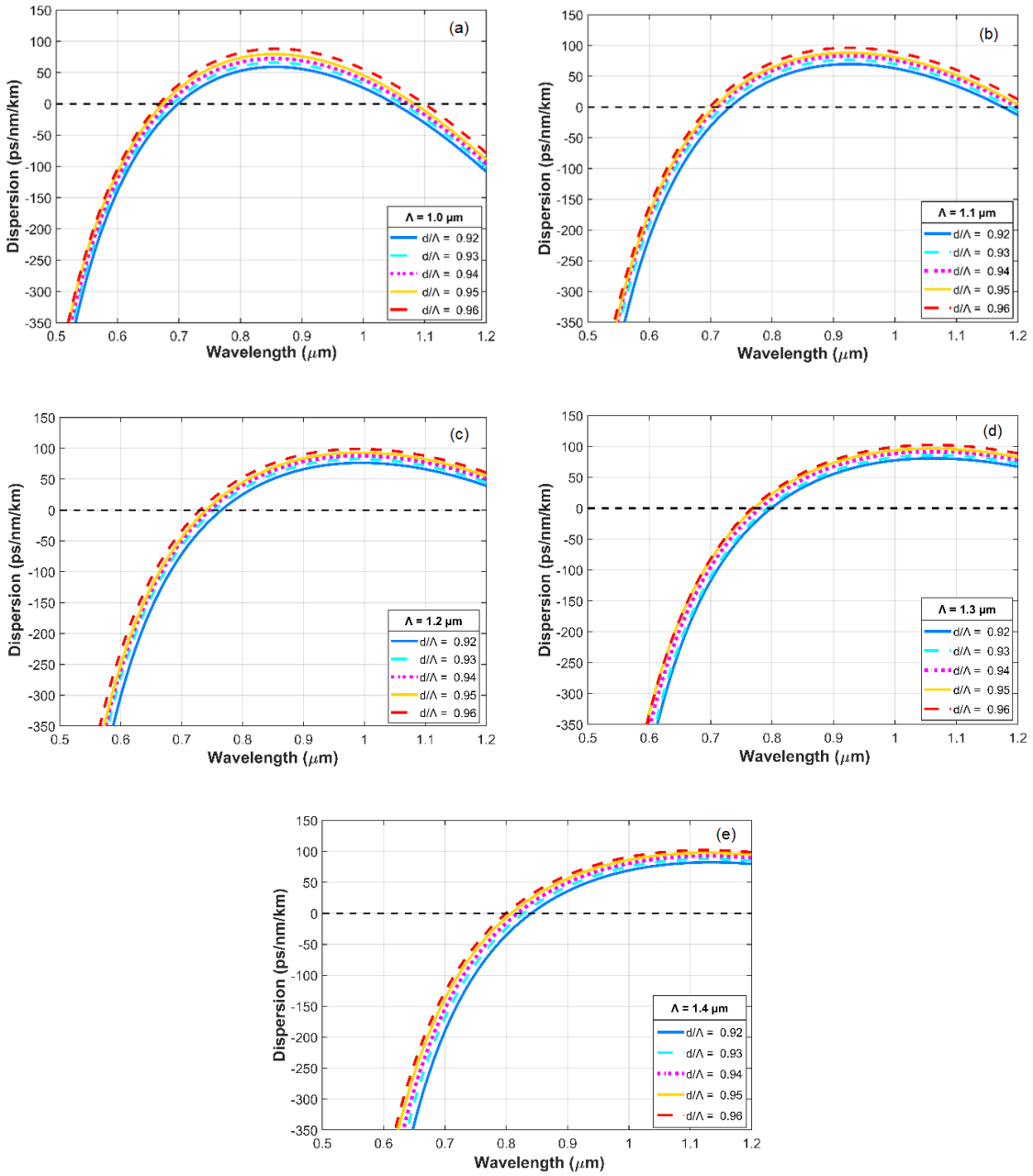

Fig. 6. The dispersion of the PCFs corresponds to the lattice constant a) $\Lambda = 1.0\ \mu$m ; b) $\Lambda = 1.1\ \mu$m ; c) $\Lambda = 1.2\ \mu$m; d) $\Lambda = 1.3\ \mu$m and e) $\Lambda = 1.4\ \mu$m with filling factor varying from 0.92 to 0.96.

#F_2 has a lattice constant $\Lambda = 1.4\ \mu$m and a filling factor $d/\Lambda = 0.92$, with a zero dispersion wavelength ZDW $= 0.835\ \mu$m . This fiber is intended for SCG in the anomalous dispersion regime with a pump wavelength of 850 nm. The dispersion value is 10.6 ps/nm/km at the pump wavelength.

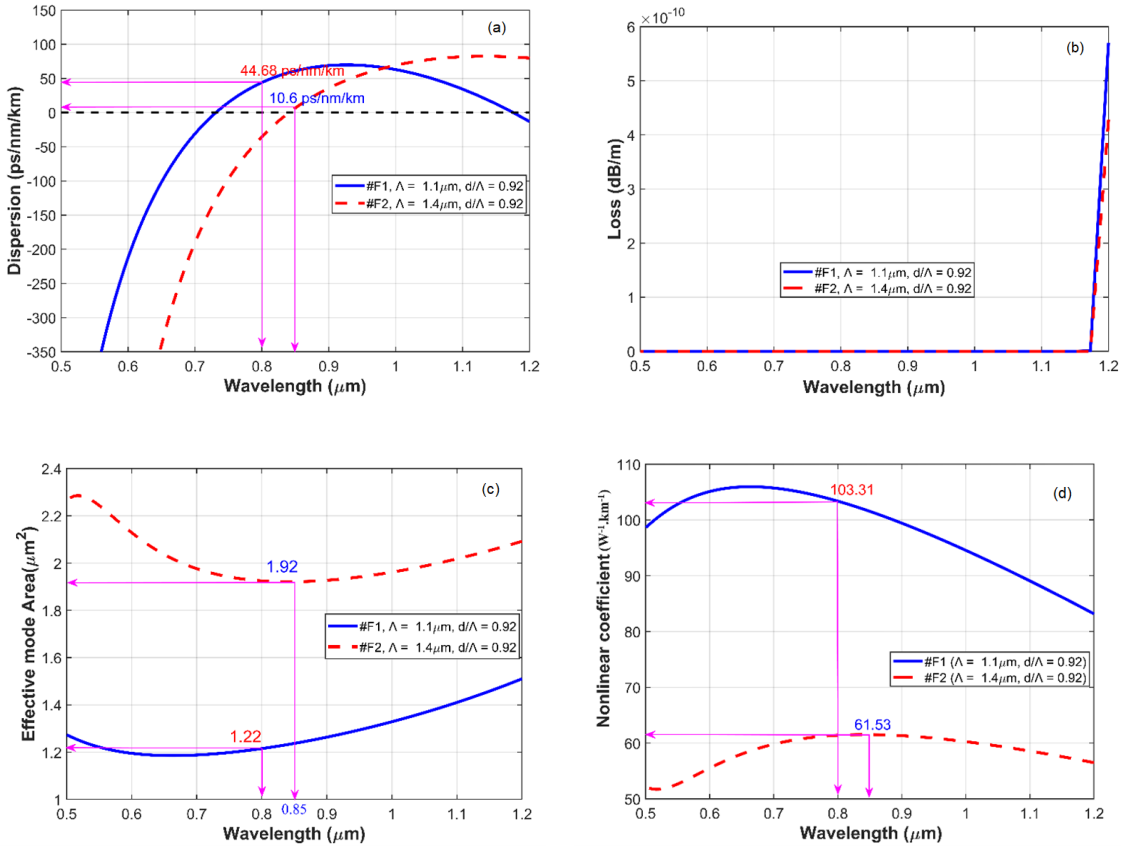

Fig. 7. Characteristic properties of two optimized fibers for supercontinuum generation: (a) dispersion; (b) confinement loss; (c) effective mode area; and (d) nonlinear coefficient.

Figure 7b shows the confinement loss characteristics of the optimal fiber bottle. In the wavelength range from 0.5 μm to 1.15 μm , there is not much difference in the values of the two optimal fibers. In the investigated wavelength region, the confinement loss of the two optimal fibers almost coincides with the horizontal axis, and has a small confinement loss value compared to the previous works in Table 2. At the pumping wavelength, the confinement loss values of fibers #F_1 and #F_2 aredB/m and dB/m, respectively. Low confinement loss is an outstanding feature of our structure compared to previous constructions.

Figures 7c and 7d present the effective mode area (A_{eff}) and nonlinear coefficient (γ) of the two proposed fibers. Fibers #F_1 and #F_2 have almost the same curve, in which the effective mode area of fiber #F_2 is higher than fiber #F_1. Because the nonlinear coefficient is inversely proportional to the effective mode area (Eq. (4)), the nonlinear coefficient of fiber #F_1 is larger than fiber #F_2 in the wavelength region investigated. Highly nonlinear PCF is most desirable for SCG produced with input energies as low as pico joules (pJ).

Table 2 presents the values of fiber property quantities proposed in this work compared with previous works [34–36]. From those results, the effective mode area of fiber #F_1 is small

Table 2. The values of characterizing quantities are calculated at pumping wavelength of the proposed PCFs.

#	Pump wavelength (nm)	D $[\text{ps.(nm.km)}^{-1}]$	A_{eff} (μm^2)	γ $(\text{W}^{-1}.\text{km}^{-1})$	L_c (dB/m)
# F_1	800	44.68	1.22	103.31	-1.32×10^{-15}
# F_2	850	10.6	1.92	61.53	8.15×10^{-16}
Water [34]	1300	-0.0114	2.089	69.4	1.63×10^{-7}
Ethanol [34]	1300	-0.011	1.965	73.8	3.55×10^{-8}
Benzene [34]	1300	-0.0124	1.521	95.4	6.76×10^{-11}
C_2Cl_4 [35]	1560	3.2	16.670	40.79	5.3
CCl_4 [36]	1030	-85	42.2	22.1	-

at 1.22 μm^2, while at the pump wavelength of 850 nm, this value is 1.92 μm^2 of fiber #F_2. We can see that the effective mode area in our construction is much smaller than in other publications. Furthermore, the confinement loss value in our study was many times smaller than the compared fibers [34–36]. The results obtained demonstrate that these PCFs are suitable for SCG applications.

4. Conclusion

In this paper, we designed a new photonic crystal fiber with a core filled with heavy water. Such a PCF is common, environmentally friendly, and has a low nonlinear refractive index compared to silica. This is a new point of the article compared to previous works. Although the work uses materials with a low refractive index, with the designed structure, light still is guided in the core according to the phenomenon of total internal reflection. The properties of hexagonal lattice PCFs are controlled by the variation of the filling factor and the lattice constant. The properties including effective mode area, nonlinear coefficient, dispersion, and loss of the proposed fiber are also studied. We have proposed two optimal fibers #F_1 ($\Lambda = 1.1$ μm, $d/\Lambda = 0.92$) and #F_2 ($\Lambda = 1.4$ μm, $d/\Lambda = 0.92$) with flat dispersion, small effective mode area, and low confinement loss compared to some previous works. The proposed fibers have a promising value for SCG. The flexibility of these structures opens the door for a multitude of applications across diverse domains, including high-speed communications, ultrafast lasers, and advanced sensors.

Acknowledgment

This research is funded by Vietnam's Ministry of Education and Training (B2023-TDV-07).

References

[1] J. C. Knight, T. A. Birks, P. St. J. Russell and D. M. Atkin, *All-silica single-mode optical fiber with photonic crystal cladding*, Opt. Lett. **21** (2020) 1547.

[2] T. A. Birks, J. C. Knight and P. St. J. Russell, *Endlessly single-mode photonic crystal fiber*, Opt. Lett. **22** (1997) 961.

[3] J. C. Knight, J. Arriaga, T. A. Birks, A. Ortigosa-Blanch, W. J. Wadsworth, P. St. J. Russell, *Anomalous dispersion in photonic crystal fiber*, IEEE Photonics Technol. Lett. **12** (200) 807.

[4] A. Ortigosa-Blanch, J. C. Knight, W. J. Wadsworth, J. Arriaga, B. J. Mangan, T. A. Birks and P. St. J. Russell, *Highly birefringent photonic crystal fibers*, Opt. Lett. **25** (2000) 1325.

[5] V. Finazzi, T. M. Monro and D. J. Richardson, *Small-core silica holey fibers: nonlinearity and confinement loss trade-offs*, J. Opt. Soc. Am. B **20** (2003) 1427.

[6] W. J. Wadsworth, A. O. Blanch, J. C. Knight, T. A. Birks, T. P. M. Man and P. St. J. Russell, *Supercontinuum generation in photonic crystal fibers and optical fiber tapers: a novel light source*, Journal of the Optical Society of America B **19** (2002) 2148.

[7] S. Dupont, C. Petersen, J. Thøgersen, C. Agger, O. Bang and S. R. Keiding, *IR microscopy utilizing intense supercontinuum light source*, Opt. Express **20** (2012) 4887.

[8] K. Ke, C. Xia, M. N. Islam, M. J. Welsh and M. J. Freeman, Mid-infrared absorption spectroscopy and differential damage in vitro between lipids and proteins by an all-fiber-integrated supercontinuum laser, Opt. Express **17** (2009) 12627.

[9] C. R. Petersen, N. Prtljaga, M. Farries, J. Ward, B. Napier, G. R. Lloyd, J. Nallala, N. Stone and O. Bang, *Mid-infrared multispectral tissue imaging using a chalcogenide fiber supercontinuum source*, Opt. Lett. **43** (2018) 999.

[10] B. Liu, M. Hu, X. Fang, Y. Wu, Y. Song, L. Chai, C. Wang and A. Zheltikov, *High-power wavelength-tunable photonic-crystal-fiber based oscillator-amplifier-frequency-shifter femtosecond laser system and its applications for material microprocessing*, Laser Phys. Lett. **6** (2009) 44.

[11] T. Udem, R. Holzwarth and T. W. Hänsch, *Optical frequency metrology*, Nature **416** (2002) 233.

[12] R. Buczynski, D. Pysz, R. Stepien, A. J. Waddie, I. Kujawa, R. Kasztelanic, M. Franczyk and M. R. Taghizadeh, *Supercontinuum generation in photonic crystal fibers with nanoporous core made of soft glass*, Laser Phys. Let. **8** (2011) 443.

[13] J. K. Ranka, R. S. Windeler and A. J. Stentz, *Visible continuum generation in air-silica microstructure optical fibers with anomalous dispersion at 800 nm*, Opt. Lett. **25** (2000) 25.

[14] J. M. Dudley, L. Provino, N. Grossard, H. Maillotte, R. S. Windeler, B. J. Eggleton and S. Coen, *Supercontinuum generation in air-silica microstructured fibers with nanosecond and femtosecond pulse pumping*, J. Opt. Soc. Am. B **19** (2002) 765.

[15] K. D. Xuan, L. C. Van, Q. H. Dinh, L. V. Xuan, M. Trippenbach, R. Buczynski, *Dispersion characteristics of a suspended-core optical fiber infiltrated with water*, Appl. Opt. **56** (2017) 1012.

[16] H. V. Le, V. L. Cao, H. T. Nguyen, A. M. Nguyen, R. Buczyński and R. Kasztelanic, *Application of ethanol infiltration for ultraflattened normal dispersion in fused silica photonic crystal fibers*, Laser Phys. **28** (2018) 115106.

[17] P. Zhao, M. Reichert, S. Benis, D. J. Hagan and E. W. V. Stryland, *Temporal and polarization dependence of the nonlinear optical response of solvents*, Optica **5** (2018) 583.

[18] R. Zhang, J. Teipel and H. Giessen, *Theoretical design of a liquid-core photonic crystal fiber for supercontinuum generation*, Opt. Express **14** (2006) 6800.

[19] R. Raei, M. Ebnali-Heidari and H. Saghaei, *Supercontinuum generation in organic liquid-liquid core-cladding photonic crystal fiber in visible and near-infrared regions*, J. Opt. Soc. Am. B **35** (2018) 323.

[20] L. C. Van, A. Anuszkiewicz, A. Ramaniuk, R. Kasztelanic, K. X. Dinh, M Trippenbach and R Buczynski, *Supercontinuum generation in photonic crystal fibers with core filled with toluene*, J. Opt. **19** (2017) 125604.

[21] L. C. Van and T. D. Van, *Broadband supercontinuum generation with low peak power in controllable C_7H_8-core photonic crystal fibers of characteristic quantities*, Indian J. Phys. **3** (2023) 1061.

[22] C. V. Lanh, V. T. Hoang, V. C. Long, K. Borzycki, K. D. Xuan, V. T. Quoc, M. Trippenbach, R. Buczyński and J. Pniewski, *Optimization of optical properties of photonic crystal fibers infiltrated with chloroform for supercontinuum generation*, Laser Phys. **29** (2019) 075107.
[23] L. C. Van, V. T. Hoang, V. C. Long, K. Borzycki, K. D. Xuan, V. T. Quoc, M. Trippenbach, R. Buczyński and J. Pniewski, *Supercontinuum generation in photonic crystal fibers infiltrated with nitrobenzene*, Laser Phys. **30** (2020) 035105.
[24] T. D. Van, L. C. Van, *Supercontinuum generation in $C_6H_5NO_2$-core photonic crystal fibers with various air-hole size*, Modern Physics Letters B **37** (2023) 2350063.
[25] V. T. Dang and V. L. Chu, *Design and optimization of $C_6H_5NO_2$-core photonic crystal fibers of broadband supercontinuum generation with low peak power*, Cryst. Res. Technol. **58** (2023) 2300085.
[26] Lumerical MODE Solutions - Informer Technologies, Inc. (available at: https://lumerical-mode-solutions.software.informer.com/).
[27] D. Churin, T. N. Nguyen, K. Kieu, R. A. Norwood and N. Peyghambarian, *Mid-IR supercontinuum generation in an integrated liquid-core optical fiber filled with CS_2*, Opt. Mat. Express **3** (2013) 1358.
[28] L.C. Van, B. T. L. Tran, T. D. Van, N. V. T. Minh, T. N. Thi, H. P. N. Thi, M. H. T. Nguyen and V. T. Hoang, *Supercontinuum generation in highly birefringent fiber infiltrated with carbon disulfide*, Opt. Fiber Technol. **75** (2023) 103151.
[29] S. Kedenburg, M. Vieweg, T. Gissibl and H. Giessen, *Linear refractive index and absorption measurements of nonlinear optical liquids in the visible and near-infrared spectral region*, Opt. Mat. Express **2** (2012) 1588.
[30] H. Odhner and D. T. Jacobs, *Refractive index of liquid D_2O for visible wavelengths*, J. Chem. Eng. Data **57** (2102) 166.
[31] A. S. L. Gomes, E. L. Falcão-Filho, C. B. de Araújo, D. Ratativa and R. E. de Araújo, *Thermally managed eclipse Z-scan*, Opt. Express **15** (2007) 1712.
[32] C. Z. Tan, *Determination of refractive index of silica glass for infrared wavelengths by IR spectroscopy*, J. Non-Cryst. Solids **223** (1998) 158.
[33] P. Dhara and V. K. Singh, *Investigation of rectangular solid-core photonic crystal fiber as temperature sensor*, Microsyst. Technol. **27** (2021) 127.
[34] A. M. Maili, I. Yakasai, P. E. Abas, M. M. Nauman, R. A. Apong *et al.*, *Design and simulation of photonic crystal fiber for liquid sensing*, Photonics **8** (2021) 16.
[35] H. V. Le, V. T. Hoang, H. T. Nguyen, V. C. Long, R. Buczynski, R. Kasztelanic, *Supercontinuum generation in photonic crystal fibers infiltrated with tetrachloroethylene*, Opt. Quant. Electron. **53** (2021) 187.
[36] V. T. Hoang, R. Kasztelanic, A. Filipkowski, G. Stępniewski, D. Pysz, M. Klimczak, S. Ertman, V. C. Long, T. R. Woliński, M. Trippenbach, K. D. Xuan, M. Śmietana, R. Buczyński, *Supercontinuum generation in an all-normal dispersion large core photonic crystal fiber infiltrated with carbon tetrachloride*, Opt. Mater. Exp. **9** (2019) 2264.